Influence of internal electric fields on bonding and properties of impurities in insulators: Mn^{2+} in $LiBaF_3$ and normal perovskites

A. Trueba,[1] J. M. García-Lastra,[2] M. T. Barriuso,[3] J. A. Aramburu,[1] and M. Moreno[1]

[1]*Departamento de Ciencias de la Tierra y Física de la Materia Condensada, Universidad de Cantabria,*
Avda. de los Castros s/n. 39005 Santander, Spain

[2]*Departamento de Física de Materiales, Facultad de Químicas, Universidad del País Vasco, 20018 San Sebastián, Spain*

[3]*Departamento de Física Moderna, Universidad de Cantabria,*
Avda. de los Castros s/n. 39005 Santander, Spain

Although in $LiBaF_3:Mn^{2+}$ the impurity replaces Li^+ thus forming octahedral MnF_6^{4-} units the experimental hyperfine and anisotropic superhyperfine constants and the energies of *d-d* optical transitions do not fit into the pattern observed for Mn^{2+}-doped normal perovskite lattices. Seeking to look into this relevant issue first-principles calculations in the framework of the density-functional theory have been carried out for MnF_6^{4-} complexes embedded in both $KMgF_3$ and $LiBaF_3$ host lattices which display normal and inverted perovskite structures respectively. The present calculations lead to a value of the equilibrium Mn^{2+}-F^- distance, R_I, which is the same for both host lattices within 0.015 Å. Despite this fact and in agreement with experimental data the calculated values of both the anisotropic superhyperfine constant, A_p, and the cubic-field splitting parameter, 10Dq, for $LiBaF_3:Mn^{2+}$ are found to be higher than those for $KMgF_3:Mn^{2+}$ while Racah parameters are a bit higher for the latter case. All these results, and also the 3% reduction undergone by the hyperfine constant on passing from $KMgF_3:Mn^{2+}$ to $LiBaF_3:Mn^{2+}$ are shown to be connected with a parallel increase in the covalency. These surprising results, which cannot be ascribed to a different R_I value, are shown to arise from the internal electric field, $\mathbf{E}_R$, due to all lattice ions lying outside the MnF_6^{4-} complex. Although, according to symmetry, $\mathbf{E}_R$ is null at Mn^{2+} site this is shown to be not true in the neighborhood of ligands for the $LiBaF_3$ host lattice. The quite different shape of $\mathbf{E}_R$ in normal and inverted perovskite lattices is shown to be already understood considering only the first two shells surrounding the MnF_6^{4-} complex. The present results demonstrate that the traditional ligand field theory fails to understand the changes undergone by optical and magnetic parameters of a complex when a host lattice is replaced by another one which is not *isomorphous*. The relevance of present conclusions for understanding the color of Cr^{3+}-based gemstones is also underlined.

I. INTRODUCTION

A great simplification for understanding the electronic properties of insulating compounds containing a transition-metal cation, M, is gained through the concept of complex.[1–3] In agreement with this idea the optical properties of compounds such as $CoCl_3(NH_3)_6$ or $KMnF_3$ can be explained to a good extent considering only the MX_N complex formed by the transition-metal cation with the N nearest neighbor anions or ligands. The usefulness of the concept of complex is greatly supported, for instance, by the comparison of optical spectra of $KMnF_3$ or $RbMnF_3$ pure compounds[4,5] with those measured for Mn^{2+}-doped cubic fluoroperovskites where MnF_6^{4-} complexes are truly diluted in the corresponding host lattices.[6,7] The *d-d* electronic transitions displayed by all these systems look very similar indeed.

Bearing in mind this kind of experimental evidence it is assumed within the traditional ligand field theory (LFT) that the electronic properties of a transition-metal impurity in an insulating lattice essentially depend on: a) The nature of the impurity and ligands; b) The number and geometrical arrangement of ligands; c) The actual distance between ligands and the impurity.

In agreement with this widely accepted standpoint, if the same MX_N complex is inserted in two different lattices, the possible differences encountered when comparing the optical or the electron-paramagnetic-resonance (EPR) spectra should then be ascribed to a change of metal-ligand distances. This statement has been well verified for Mn^{2+}-, Ni^{2+}-, and Fe^{3+}-doped cubic fluoroperovskites, Cr^{3+}- and Fe^{3+}-doped cubic elpasolites and also in the case of Mn^{2+}-doped fluorite-type lattices.[8–13] In all these systems the variation of optical-absorption (or excitation) maxima and the spin-Hamiltonian parameters of the complex through different host lattices can be well accounted for by the change of the *equilibrium* impurity-ligand distance, R_I, at ambient pressure. This distance follows in turn the value of the cubic lattice parameter, *a*, along the series of *isomorphous* host lattices. In the same vein, the changes of optical properties induced by a hydrostatic pressure on $Cs_2NaScCl_6:Cr^{3+}$ (Ref. 14) can also be well explained on the basis of the progressive reduction in the Cr^{3+}-Cl^- distance.[15]

Despite the variations of optical and magnetic properties due to a complex in a series of *isomorphous* host lattices is well understood by means of the traditional LFT, recent experimental results stress that this is no longer true when comparing the same complex embedded in two lattices with *different* crystal structure. A relevant example in this domain concerns ruby and emerald whose color comes from a slightly distorted CrO_6^{9-} complex embedded in Al_2O_3 and $Be_3Si_6Al_2O_{18}$ lattices, respectively.[16,17] Recent measure-
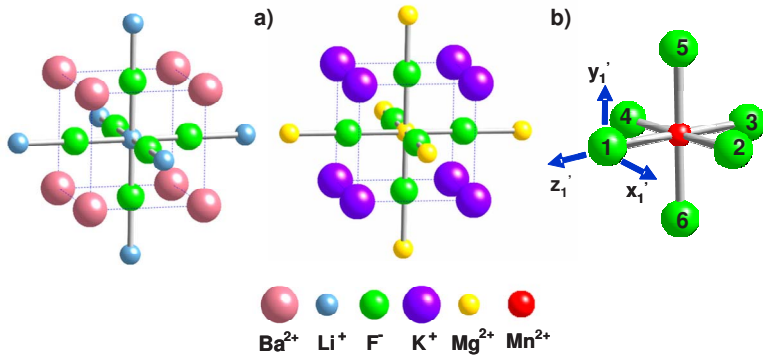
FIG. 1. (Color online) a) 21 atom clusters used in the calculations of the inverted $BaLiF_3$ (left) and normal $KMgF_3$ (right) perovskite structures. Unit cells are marked with dashed lines. The lattice constant a is thus equal to $2R_0$. Similar clusters were used for the calculations of the corresponding Mn^{2+} impurity centers but replacing the central ion (Li^+ in $LiBaF_3$ and Mg^{2+} in $KMgF_3$) by Mn^{2+}. b) MnF_6^{4-} complex and arrangement of local axes for ligand 1 placed on the x axis.

ments have shown that, within the experimental uncertainty (± 1 pm), the average Cr^{3+}-O^{2-} distance is the same for both gemstones.[18,19] Therefore, the red and green colors exhibited by ruby and emerald, respectively, can hardly be accounted for on the basis of the traditional LFT. This surprising situation has been pointed out to be reasonably understood once the electric field created by the rest of lattice ions upon the CrO_6^{9-} complex, $\mathbf{E}_R(\mathbf{r})$, is also taken into consideration.[20,21] This statement just means that, although active electrons are essentially localized in the complex, the associated optical and magnetic properties cannot be fully understood considering only such a complex *in vacuo*. According to this view the cubic-field splitting parameter, 10Dq, which is behind the color of Al_2O_3:Cr^{3+} and $Be_3Si_6Al_2O_{18}$:Cr^{3+}, depends on the metal-ligand distance but *also* on the shape of $\mathbf{E}_R(\mathbf{r})$ in the complex region which in turn reflects the host-lattice structure.

Despite the influence of $\mathbf{E}_R(\mathbf{r})$ on the actual value of 10Dq has been investigated for different gemstones doped with Cr^{3+}, no attention has been paid up to now to the changes that such internal electric field introduces on the bonding inside the complex. To look into this issue is certainly relevant because hyperfine (HF) and superhyperfine (SHF) tensors as well as the Racah parameters do depend on the degree of covalency existing in the transition-metal complex.[1,2]

The present work is mainly addressed to explore this subject. More specifically, this study is focused on the different spectroscopic properties exhibited by a Mn^{2+} impurity placed in the inverted perovskite lattice $LiBaF_3$ or in host lattices with a normal perovskite structure. Both structures are depicted in Fig. 1. Main reasons for this choice are the following:

1) Electron nuclear double-resonance (ENDOR) data[22,23] clearly prove that in $LiBaF_3$ the Mn^{2+} impurity replaces a Li^+ ion of the host matrix thus leading to the formation of an octahedral MnF_6^{4-} complex with remote charge compensation. Such a complex is thus the same than that formed in normal perovskite lattices (such as $KMgF_3$) where the Mn^{2+} impurity occupies the position of the divalent cation Mg^{2+}.[24–30]

2) The existence of ENDOR measurements[23] carried out on $LiBaF_3$:Mn^{2+} allows a precise comparison of hyperfine and superhyperfine parameters with those measured for Mn^{2+}-doped $KZnF_3$, $CsCdF_3$, and $CsCaF_3$ using the same tool. It was early noted that both the HF and the anisotropic SHF constant of $LiBaF_3$:Mn^{2+} can hardly be fitted into the

pattern for Mn^{2+} impurities in normal perovskites.[22,31]

3) The excitation spectrum of $LiBaF_3$:Mn^{2+} has recently been measured.[32] Despite the lattice constant, a, of $KMgF_3$ (Ref. 33) and $LiBaF_3$ (Ref. 34) lattices is the same within 0.3%, there are significant differences between the excitation spectra corresponding to MnF_6^{4-} embedded in the two referred lattices.[7,32]

4) As both the normal and the inverted perovskite lattices are cubic, it is easier to explore in detail the nature of antibonding e_g ($\sim x^2-y^2$, $3z^2-r^2$) and t_{2g} ($\sim xy, xz, yz$) orbitals (where unpaired electrons are located in the ground state) than in systems with much lower local symmetry such as it happens for instance in the case of ruby.[16–21] For these reasons $LiBaF_3$:Mn^{2+} and $KMgF_3$:Mn^{2+} can be considered as model systems.

5) Bearing in mind that active electrons in these systems are highly localized[8,35] relatively small clusters can be used for calculating the ground-state equilibrium distance and the associated magnetic and optical parameters. In all cases the influence of the electrostatic potential coming from ions outside the cluster is taken into consideration.

Apart from these reasons, it is worthwhile to remark that a significant attention has been paid in the last years to $LiBaF_3$ material doped with transition metal or rare-earth impurities in the search of new systems for application as devices in the deep ultraviolet or scintillators.[36–38]

Seeking to explore the variations in covalency of the MnF_6^{4-} unit on passing from a normal perovskite lattice to $LiBaF_3$ first-principles calculations in the framework of the density-functional theory (DFT) have been carried out. For the sake of clarity, the value of R_I, the electronic density in antibonding e_g and t_{2g} orbitals, and significant spectroscopic parameters calculated for $LiBaF_3$:Mn^{2+} are compared with those derived for $KMgF_3$:Mn^{2+}.

In the realm of spectroscopic parameters, attention is firstly focused on HF and SHF tensors. In particular, it is explored whether the differences between HF and SHF tensors measured[22–25] for $LiBaF_3$:Mn^{2+} and $KMgF_3$:Mn^{2+} can or not be accounted for on the basis of distinct R_I values. Subsequently, the connection between such experimental differences and the corresponding changes in chemical bonding is analyzed in detail. In a second step, attention is paid to two optical parameters measured for $LiBaF_3$:Mn^{2+}, 10Dq and the energy of the relatively sharp $^6A_1 \rightarrow {}^4A_1$, ^4E crystal-field peak.[32] Both of them are somewhat *anomalous* when compared to the corresponding figures found for Mn^{2+} in normal perovskites.[6,7]

TABLE I. Experimental hyperfine, A, and superhyperfine, A_s and A_p, parameters (all given in megahertz) for MnF_6^{4-} placed in the inverted perovskite $LiBaF_3$ lattice as well as in a series of cubic fluoroperovskites. Superhyperfine parameters have been measured at 4.2 K by ENDOR for $KZnF_3$, $CsMF_3(M=Cd,Ca)$ and $LiBaF_3$ doped with Mn^{2+} while the hyperfine constant has been obtained by this technique only for $CsCaF_3:Mn^{2+}$ and $LiBaF_3:Mn^{2+}$. EPR data correspond to room temperature. Experimental errors are given in parenthesis. Values of $R_0=a/2$ (Refs. [33] and [34]) and the equilibrium Mn^{2+}-F^- distance, R_I, (taken from Ref. [8]) are also included for comparison purposes. Both R_0 and R_I are given in Å.

Host	R_0	R_I	$\|A\|$	A_p	A_s	Technique	Ref.
$LiBaF_3$	1.998		265.324 (0.003)	11.0 (0.1)	55.4 (0.1)	ENDOR	23
$KMgF_3$	1.993	2.06	273 (1.5)	5.9 (1.5)	54.3 (2)	EPR	24 and 25
$KZnF_3$	2.027	2.08	272.4 (0.3)	9.12 (0.03)	54.3 (0.03)	ENDOR	26
$CsCdF_3$	2.232	2.15	271.2 (0.6)	7.44 (0.9)	42.45 (0.9)	EPR	27
$CsCdF_3$	2.232	2.15		8.17 (0.04)	43.97 (0.04)	ENDOR	28
$CsCaF_3$	2.262	2.16	276.734 (0.005)	8.72 (0.1)	40.75 (0.1)	ENDOR	29

The present work is arranged as follows. Section II provides with a detailed analysis of relevant experimental data available for Mn^{2+} impurities in normal perovskite lattices and in $LiBaF_3$. This study will clarify what are the main differences lying well beyond experimental uncertainties. In Sec. III the computational details are reported, while in Sec. IV the relevant results obtained on $LiBaF_3:Mn^{2+}$ and $KMgF_3:Mn^{2+}$ are displayed and discussed in some detail. In Sec. IV particular attention is paid to the shape of the electrostatic potential, $V_R(\mathbf{r})$, associated with $\mathbf{E}_R(\mathbf{r})$, in both normal and inverted perovskite lattices and especially to its influence on the covalency of embedded MnF_6^{4-} units. Finally, the relevance of the present conclusions for other systems is shortly outlined in Sec. V.

II. Mn^{2+} IN NORMAL AND INVERTED PEROVSKITE LATTICES. RELEVANT EXPERIMENTAL DATA

A. Hyperfine and superhyperfine tensors

For an octahedral MnF_6^{4-} complex in its $^6A_1(t_{2g}^3 e_g^2)$ ground state, the terms in the spin Hamiltonian describing the HF and SHF interactions are written as[39]

$$H_{HF} = A\mathbf{IS} + \sum_{k=1}^{6} \mathbf{I}[\mathbf{T}_k]\mathbf{S}. \qquad (1)$$

In Eq. (1) A denotes the HF constant while $[\mathbf{T}_k]$ ($k=1,\ldots,6$) mean the SHF tensors associated with the six ligands. In an octahedral complex the symmetry operations leaving invariant a given ligand display a tetragonal C_{4v} group. Therefore, a diagonalized $[\mathbf{T}_k]$ tensor involves two different components called $T_\parallel$ and $T_\perp$. Principal directions for the SHF tensor of one of ligands are shown on Fig. 1. The $T_\parallel$ component is associated with the corresponding metal-ligand direction. For practical purposes, instead of analyzing directly $T_\parallel$ and $T_\perp$ parameters, it is often more useful to work with the quantities A_p and A_s, defined by

$$T_\parallel = A_s + 2A_p; \quad T_\perp = A_s - A_p. \qquad (2)$$

Microscopically, A_p reflects mainly the admixture of $3d$ orbitals coming from Mn^{2+} with $2p$ valence orbitals of F^-,

which is allowed for both e_g and t_{2g} antibonding orbitals.[1,3,39] By contrast, A_s mainly comes from the $2s(F^-)-3d(Mn^{2+})$ admixture which is only allowed for the two e_g orbitals. As for free F^- ion, the $2s$ orbital lie 23 eV below the $2p$ orbital, bonding in a e_g level is, however, mainly established through $2p(F^-)$ orbitals.[40]

Representative values of A, A_p, and A_s parameters derived from magnetic-resonance measurements for MnF_6^{4-} in normal cubic perovskite lattices and in $LiBaF_3$ are gathered on Table I, together with the values of $R_0=a/2$ and R_I distances. In such a table, ENDOR results are included when available due to its higher accuracy with respect to normal EPR data. The SHF tensor has been measured by ENDOR at low temperature for the cubic $KZnF_3$, $CsCdF_3$, and $CsCaF_3$ lattices doped with Mn^{2+} [26,28,29] as well as for $LiBaF_3:Mn^{2+}$.[23] Interestingly, ENDOR values of A have been derived for both $CsCaF_3:Mn^{2+}$ (Ref. 29) and $LiBaF_3:Mn^{2+}$.[23]

As shown in Table I, experimental values of $|A|$ for Mn^{2+}-doped normal cubic perovskites are all lying in the 271–277 MHz region. This slight dependence of $|A|$ on the host lattice reflects that for an octahedral Mn^{2+} complex, the hyperfine constant comes from the polarization of inner $1s$, $2s$, and $3s$ orbitals by the five unpaired d electrons.[39] In a previous study[41] it was concluded that $|A|$ should increase slightly with the Mn^{2+}-F^- distance, $d|A|/dR$ being around 0.5 MHz/pm. Looking at Table I one realizes that the value $|A|$ $=265.3$ MHz measured for $LiBaF_3:Mn^{2+}$ is certainly not in the range of values reported for normal cubic perovskites. In particular, it is clearly smaller than the figure measured for $KMgF_3:Mn^{2+}$ although only by about 3%.

A more remarkable difference comes out when comparing A_p values for MnF_6^{4-} in normal perovskites with that measured for $LiBaF_3:Mn^{2+}$. As shown in Table I the A_p value measured by ENDOR for Mn^{2+}-doped $KZnF_3$, $CsCdF_3$, and $CsCaF_3$ are nearly identical all of them lying in the range 8.2–9.1 MHz. A different situation holds as regards A_s. In fact, A_s increases by 35% on passing from $CsCaF_3:Mn^{2+}$ to $KMgF_3:Mn^{2+}$. This significant increase has been proved to reflect the strong dependence of A_s upon R.[8,40] The reason why A_p is much less dependent on R has been explained previously.[10,40,42]

Bearing in mind the experimental A_p values measured for Mn^{2+} in normal perovskites it seems again not easy to un-

TABLE II. Experimental values of the energies corresponding to $^6A_{1g} \rightarrow {}^4A_{1g}$ and $^6A_{1g} \rightarrow {}^4A_{1g}, {}^4E_g$ transitions (denoted as E_1 and E_3, respectively) measured for AMnF$_3$ ($A=K,Rb$) pure compounds and also for the Mn^{2+} impurity embedded in a series of normal cubic fluoroperovskites. These results are compared with the corresponding values found for LiBaF$_3$:Mn^{2+}. E_1 and E_3 are given in cm^{-1}. For the sake of clarity available values of R_0 and R_I distances (given in Å) are also included in the table.

System	R_0	R_I	E_1	E_3	$E_3 - E_1$	Ref.
LiBaF$_3$:Mn^{2+}	1.998		16129	24096	7967	32
KMgF$_3$:Mn^{2+}	1.993	2.06	18240	25200	6960	6 and 7
KZnF$_3$:Mn^{2+}	2.027	2.08	18530	25210	6680	6
KMnF$_3$	2.095	2.095	18900	25245	6345	4 and 5
RbMnF$_3$	2.120	2.12	19300	25275	5975	4 and 5
RbCdF$_3$:Mn^{2+}	2.20	2.13	19530	25230	5700	6
CsCaF$_3$:Mn^{2+}	2.262	2.16	19860	25380	5520	6 and 7

derstand the value $A_p = 11 \pm 0.1$ MHz reported for LiBaF$_3$:Mn^{2+} (Ref. 23) which is about 30% higher than the A_p value derived for KZnF$_3$:Mn^{2+}.[26] The results collected in Table I stress that such a difference can hardly be accounted for on the basis of the actual value of the Mn^{2+}-F$^-$ distance.

B. Crystal field transitions

The so-called *d-d* or crystal-field transitions for an octahedral d^5 complex with $S=5/2$ in the ground state are both parity and spin forbidden. For this reason the crystal-field transitions for MnF$_6^{4-}$ complexes are observed by means of the optical-absorption technique for pure compounds such as KMnF$_3$ or RbMnF$_3$ (Refs. 4 and 5) while for doped systems such transitions are usually measured through the excitation spectrum of the $^4T_{1g}(t_{2g}^4 e_g^1) \rightarrow {}^6A_1(t_{2g}^3 e_g^2)$ emission.[6,7] Among the crystal-field transitions observed for Mn^{2+} in normal perovskites and in LiBaF$_3$, values corresponding to the first $^6A_1(t_{2g}^3 e_g^2) \rightarrow {}^4T_{1g}(t_{2g}^4 e_g^1)$ transition (whose energy is termed E_1) and the third $^6A_{1g}(t_{2g}^3 e_g^2) \rightarrow {}^4A_{1g}, {}^4E_g(t_{2g}^3 e_g^2)$ transition (whose energy is termed E_3) are both gathered in Table II. For the sake of completeness the values of R_0 and R_I distances are also included in such a table. While E_1 depends on 10Dq, E_3 is independent on this parameter and thus the $^6A_1(t_{2g}^3 e_g^2) \rightarrow {}^4A_{1g}, {}^4E_g(t_{2g}^3 e_g^2)$ transition plays a similar role to the $^4A_2(t_{2g}^3) \rightarrow {}^2E_g(t_{2g}^3)$ transition for Cr^{3+} in oxides.[16,17] A direct insight into 10Dq can simply be obtained looking at the value of $E_3 - E_1$ which is also reported on Table II. In a first approximation, $E_3 - E_1$ is just equal to 10Dq-C, involving the C Racah parameter.[1–3]

In the series of normal perovskites doped with Mn^{2+} it can be noticed that $E_3 - E_1$ decreases progressively on passing from KMgF$_3$:Mn^{2+} to CsCaF$_3$:Mn^{2+}. This fact has reasonably been explained[6,7] considering that under a hydrostatic pressure the dependence of 10Dq on the value of the metal-ligand distance, R, is given by the law

$$10Dq = KR^{-n}, \tag{3}$$

where the exponent n is usually found to lie in the 4–6 region.[15,40,43] If active electrons are fully localized in the MnF$_6^{4-}$ complex the same effect can be produced by placing the complex in a series of distinct isomorphous host lattices

producing different chemical pressures upon the complex. For MnF$_6^{4-}$ in cubic fluoroperovskites a value $n=4.7$ has been derived from an analysis of experimental results.[7] Interestingly, the 10Dq values measured for AMnF$_3$ ($A=K$,Rb) pure compounds[4,5] or for doped cubic fluoroperovskites[6,7] follow all of them the pattern of Eq. (3). However, the experimental value $E_3 - E_1 = 7967$ cm^{-1} for LiBaF$_3$:Mn^{2+} (Table II) can hardly be fitted into the results corresponding to normal perovskites with Mn^{2+}. In fact, while KMgF$_3$ and LiBaF$_3$ lattices have practically the same R_0 value the figure $E_3 - E_1 = 6960$ cm^{-1} reported for KMgF$_3$:Mn^{2+} is about 1000 cm^{-1} smaller than that for LiBaF$_3$:Mn^{2+}.

Along this line the E_3 value itself recently measured[32] for LiBaF$_3$:Mn^{2+} is also surprising when compared to data[4–7] for normal perovskites containing Mn^{2+}. As shown in Table II the E_3 values for AMnF$_3$ ($A=K$,Rb) compounds and Mn^{2+}-doped normal perovskites are all found to lie in the 25200–25380 cm^{-1} narrow range. By contrast, the value $E_3 = 24097$ cm^{-1} determined for LiBaF$_3$:Mn^{2+} can not again be fitted into such a pattern.

The main conclusions extracted from the simple inspection of E_1 and E_3 experimental values (Table II) is corroborated by an analysis of the six excitation peaks observed for KMgF$_3$:Mn^{2+} and LiBaF$_3$:Mn^{2+}. The energies of such transitions are given in Table III. From the analysis of such experimental transitions it is obtained 10Dq$=9673$ cm^{-1} for LiBaF$_3$:Mn^{2+} which is clearly higher than 10Dq $=7950$ cm^{-1} for KMgF$_3$:Mn^{2+}. A similar situation is found when comparing the experimental 10Dq parameter of Co^{2+} and Ni^{2+} impurities in LiBaF$_3$ and KMgF$_3$.[44–46] As regards the Racah parameters the figures $B=814$ cm^{-1} and $C=2995$ cm^{-1} extracted for LiBaF$_3$:Mn^{2+} are smaller than $B=847$ cm^{-1} and $C=3024$ cm^{-1} obtained for KMgF$_3$:Mn^{2+}. This fact supports that covalency is higher for the former than for the latter system.

III. COMPUTATIONAL DETAILS

First-principles calculations have been performed within the framework of the DFT by means of the Amsterdam density functional (ADF) code, 2006 version.[47] Exchange-

TABLE III. Comparison between calculated and experimental values of the optical transitions for Mn^{2+} impurity embedded in both $KMgF_3$ and $LiBaF_3$ lattices. Values of 10Dq and Racah parameters, B and C, are also collected in the table. All energies are given in cm^{-1}. Experimental data for $KMgF_3:Mn^{2+}$ and $LiBaF_3:Mn^{2+}$ are taken from Refs. 7 and 32.

	$KMgF_3:Mn^{2+}$		$LiBaF_3:Mn^{2+}$	
	Calculated	Experimental	Calculated	Experimental
$^6A_{1g} \rightarrow {}^4T_{1g}$	15282	18240	13228	16129
$^6A_{1g} \rightarrow {}^4T_{2g}$	19708	22640	17945	22220
$^6A_{1g} \rightarrow {}^4A_{1g}, {}^4E_g$	22815	25200	22120	24096
$^6A_{1g} \rightarrow {}^4T_{2g}$	26275	28070	25269	26666
$^6A_{1g} \rightarrow {}^4E_g$	28506	30230	27685	29411
$^6A_{1g} \rightarrow {}^4T_{1g}$	32221	32590	32044	33333
B	813	847	795	814
C	2937	3024	2834	2995
10Dq	9610	8430	10961	9795

correlation energy was computed according to the generalized gradient approximation (GGA) employing the Becke-Perdew functional.[48,49] High quality TZP basis sets (triple-zeta Slater type orbitals plus one polarization extra function) were used to describe all atoms. Core electrons ($1s$-$3p$ for Mn and K, $1s$ for F and Li, $1s$-$2p$ for Mg and $1s$-$4d$ for Ba) were kept frozen in geometry optimizations, while all-electron basis sets were used for computing EPR parameters. Following a previous study[8,35] most of results shown in this work on Mn^{2+}-doped $KMgF_3$ and $LiBaF_3$ have been derived using the 21 ion clusters $MnF_6K_8Mg_6^{16+}$ and $MnF_6Ba_8Li_6^{18+}$, respectively. This simplification comes from the fact that active electrons are lying essentially inside the MnF_6^{4-} complex. For instance, for the antibonding e_g orbital of MnF_6^{4-} embedded in $LiBaF_3$ the electronic density lying outside the cluster is found to be only 1%. Despite this fact geometry optimizations on the 57 ions clusters $MnF_6K_8Mg_6F_{24}Mg_{12}^{16+}$ and $MnF_6Ba_8Li_6F_{24}Li_{12}^{6+}$ have also been performed in order to study the influence of the cluster size upon the equilibrium Mn^{2+}-F^- distance, R_I. For having a supplementary check of the consistency of the employed method calculations on $MgF_6K_8Mg_6^{16+}$ or $LiF_6Ba_8Li_6^{18+}$ clusters related to the pure lattice, have also been carried out. In the geometry optimizations the positions of all ions, except F^- ligands, have been kept at their calculated lattice positions. This approximation is not unreasonable for present cases because both $Mg^{2+} \rightarrow Mn^{2+}$ and $Li^+ \rightarrow Mn^{2+}$ substitutions lead to a local relaxation which is always smaller than 3.5%.[8,35]

The electrostatic potential due to the rest of the lattice ions $V_R(\mathbf{r})$, was generated by means of 224 point charges at their lattice positions with charge values previously fit to reproduce the electric field of the infinite lattice using an Evjen-Ewald scheme.[50] Spin-restricted calculations were used for geometry optimizations while an unrestricted treatment was employed for the calculations of EPR tensors.

The LFT parameters (i.e., 10Dq and the two Racah parameters, B and C) have been computed through the Ligand Field DFT (LFDFT) methodology proposed by Atanasov *et al.*[51] It consists of an average of configuration (AOC) full-SCF calculation for the d electrons and in a further step the energy of every possible Slater determinant (252 in the case of a d^5 ion) is calculated in a non-SCF calculation using the orbitals obtained in the AOC procedure. The energy of all the Slater determinants can be expressed as a function the ligand field parameters and since the system is overdetermined (252 energies and only 4 parameters) a least-square minimum procedure is used to get the ligand field parameters.

IV. RESULTS FOR $LiBaF_3:Mn^{2+}$ AND $KMgF_3:Mn^{2+}$

In a first step, it is necessary to see whether the present DFT calculations are able to reproduce all *anomalies* encountered when comparing $|A|$, A_p and E_1 and E_3 values measured for MnF_6^{4-} in normal perovskites such as $KMgF_3$ with the corresponding results found for $LiBaF_3:Mn^{2+}$. A prerequisite for achieving this goal is to know the actual value of R_I for $LiBaF_3:Mn^{2+}$.

A. Equilibrium geometry for the ground state

As a test of the cluster method used through this work, the calculated Mg^{2+}-F^- and Li^+-F^- distances for $KMgF_3$ and $LiBaF_3$ pure lattices by means of clusters of 21 and 57 atoms are collected in Table IV. As shown in such a table the discrepancies with experimental R_0 values never exceed 2%. Calculated values of the equilibrium Mn^{2+}-F^- distance, R_I, for $LiBaF_3:Mn^{2+}$ and $KMgF_3:Mn^{2+}$ are also given in Table IV. The obtained value for the Mn^{2+}-F^- distance in the case of $KMgF_3:Mn^{2+}$ is close to $R_I = 2.07 \pm 0.01$ Å and 2.065 ± 0.005 Å derived from experimental A_s and 10Dq values, respectively, and to the figure $R_I = 2.057$ Å obtained in a previous calculation.[6,8,35] The results displayed in Table III confirm that, as expected, R_I in $LiBaF_3:Mn^{2+}$ and $KMgF_3:Mn^{2+}$ are the same within 0.015 Å. A similar situation has been encountered for Ni^{2+} impurity in the two $KMgF_3$ and $LiBaF_3$ lattices.[46] As pointed out in Sec. III, the R_0 and R_I calculated values gathered in Table IV have been derived using the Becke-Perdew functional.[48,49] Additional calculations employing the Becke-Lee-Yang-Parr (BLYP) functional[48,52] have also been performed. We have verified

TABLE IV. Calculated values of the Mg^{2+}-F^- distance for $KMgF_3$ and Li^--F^- distance for $LiBaF_3$ using clusters of 21 and 57 atoms. The calculated values for the Mn^{2+}-F^- distance, R_I, for both $KMgF_3$:Mn^{2+} and $LiBaF_3$:Mn^{2+} systems are also shown. For comparison purposes, the experimental R_0 values for pure lattices as well as the average R_I value inferred from the analysis of EPR and optical data for $KMgF_3$:Mn^{2+} are also displayed. All distances are given in Å.

		Calculated		Experimental	Ref.
System	Distance	21 atoms	57 atoms		
$LiBaF_3$	R_0	2.041	2.012	1.998	34
$KMgF_3$	R_0	2.013	1.988	1.933	33
$LiBaF_3$:Mn^{2+}	R_I	2.065	2.050		
$KMgF_3$:Mn^{2+}	R_I	2.063	2.038	2.065 ± 0.015	6 and 8

that the differences with respect to values given in Table IV never exceed 1%.

B. Covalency in e_g and t_{2g} antibonding orbitals

In the $^6A_1(t_{2g}^3 e_g^2)$ ground state of the MnF_6^{4-} complex there are three unpaired t_{2g} and two unpaired e_g electrons which are responsible for the EPR parameters. The normalized wave function of a t_{2g} orbital can shortly be written as[3,39,40]

$$|t_{2g}; \gamma\rangle = N_t\{|d(t_{2g}); \gamma\rangle - \lambda_{p\pi} |\chi_{p\pi}\rangle\} \quad (\gamma = xy, xz, yz).$$

(4)

Here the first term on the right describes a pure d wave function transforming like xy, xz or yz while the second term means a suitable linear combination of atomic orbitals (LCAO) involving p_π valence orbitals of six F^- ligands. The coefficients N_t^2 and $(N_t\lambda_\pi)^2$ reflect the probability of finding the electron on the central cation and on ligands, respectively. In the case of the antibonding e_g orbital, symmetry allows an admixture with $2p_\sigma$ and $2s$ orbitals of six ligands and thus the corresponding wave function is given by[3,39,40]

$$|e_g; \gamma\rangle = N_e\{|d(e_g); \gamma\rangle - \lambda_{p\sigma} |\chi_{p\sigma}\rangle - \lambda_s|\chi_{ps}\rangle\}$$

$$(\gamma = x^2-y^2, 3z^2-r^2)$$

(5)

Calculated values of N_i ($i=e,t$), $\lambda_{p\sigma}$, λ_s, and $\lambda_{p\pi}$ parameters for both $LiBaF_3$:Mn^{2+} and $KMgF_3$:Mn^{2+} are gathered in Table V. For the sake of completeness in addition to figures related to the equilibrium distance, R_I, those corresponding

to other values of the Mn^{2+}-F^- distance, R, are also reported.

Looking at the results associated either with $KMgF_3$:Mn^{2+} or $LiBaF_3$:Mn^{2+}, it can be noticed: i) $\lambda_{p\sigma}^2$ is certainly higher than λ_s^2; ii) N_i ($i=e,t$), $\lambda_{p\sigma}$ and $\lambda_{p\pi}$ are only slightly dependent upon R; iii) By contrast, the tiny quantity λ_s is quite sensitive to the actual R value. The origin of these trends, which are usually found for O_h transition-metal complexes,[31,53,54] has previously been explained.[10,40,42]

The comparison between results derived for $LiBaF_3$:Mn^{2+} with those for $KMgF_3$:Mn^{2+} is somewhat surprising. Indeed the data reported in Table V clearly show that the unpaired e_g and t_{2g} electrons spend more time on $2p(F)$ ligand orbitals for $LiBaF_3$:Mn^{2+} than in the other case. This is particularly true for the e_g orbital displaying σ bonding. In fact, on passing from $KMgF_3$:Mn^{2+} to $LiBaF_3$:Mn^{2+} $(N_e\lambda_\sigma)^2$ increases by ~0.08 while only ~0.03 in the case of $(N_t\lambda_\pi)^2$. Bearing in mind that N_i ($i=e,t$), $\lambda_{p\sigma}$ and $\lambda_{p\pi}$ are nearly independent on R for each one of the two considered systems the differences collected in Table IV cannot be explained on the basis of a distinct Mn^{2+}-F^- distance for $LiBaF_3$:Mn^{2+} and $KMgF_3$:Mn^{2+}.

C. Hyperfine and superhyperfine tensors

Representative calculated values of the anisotropic SHF constant, A_p, for $LiBaF_3$:Mn^{2+} and $KMgF_3$:Mn^{2+} are gathered in Table VI. Although for both systems A_p has a tiny dependence on R the calculated values for $LiBaF_3$:Mn^{2+} are systematically higher than those for $KMgF_3$:Mn^{2+} by about 25%. The results embodied in Table V are thus not far from

TABLE V. Calculated values of N_i ($i=e,t$), $\lambda_{p\sigma}$, λ_s and $\lambda_{p\pi}$ parameters for both $LiBaF_3$:Mn^{2+} and $KMgF_3$:Mn^{2+}. For the sake of completeness, calculated values for other Mn^{2+}-F^- distances, R (given in Å), different from equilibrium $R_I=2.06$ Å are also gathered in the table.

R	System	N_e^2	$(N_e\lambda_{p\sigma})^2$	$(N_e\lambda_s)^2$	N_t^2	$(N_t\lambda_{p\pi})^2$
2.02	$LiBaF_3$:Mn^{2+}	0.865	0.337	0.019	0.911	0.204
	$KMgF_3$:Mn^{2+}	0.914	0.252	0.024	0.941	0.165
2.06	$LiBaF_3$:Mn^{2+}	0.854	0.341	0.017	0.901	0.208
	$KMgF_3$:Mn^{2+}	0.905	0.256	0.021	0.932	0.167
2.10	$LiBaF_3$:Mn^{2+}	0.839	0.347	0.015	0.886	0.217
	$KMgF_3$:Mn^{2+}	0.894	0.261	0.018	0.920	0.173

TABLE VI. Calculated values of the anisotropic superhyperfine constant, A_p, and the hyperfine constant, A, for both $LiBaF_3:Mn^{2+}$ and $KMgF_3:Mn^{2+}$ systems. For the sake of clarity, results obtained for three different values of the Mn^{2+}-F^- distance, R, are given. Hyperfine and superhyperfine constants are given in megahertz, while Mn^{2+}-F^- distances are given in Å.

R	System	A_p	A
2.02	$LiBaF_3:Mn^{2+}$	13.2	−115.8
	$KMgF_3:Mn^{2+}$	10.7	−123.9
2.06	$LiBaF_3:Mn^{2+}$	12.6	−114.3
	$KMgF_3:Mn^{2+}$	10.4	−123.3
2.10	$LiBaF_3:Mn^{2+}$	11.95	−111.9
	$KMgF_3:Mn^{2+}$	10.0	−122.1

FIG. 2. (Color online) a) Calculated Mn^{2+}-F^- distance dependence of 10Dq parameter for both $KMgF_3:Mn^{2+}$ (dashed line) and $LiBaF_3:Mn^{2+}$ (solid line). b) The same for Racah parameter C. c) The same for B parameter.

experimental findings for A_p displayed in Table I.

The increase undergone by A_p on passing from $KMgF_3:Mn^{2+}$ to $LiBaF_3:Mn^{2+}$ is consistent with the parallel increase in covalency shown in Table V. The relation between A_p and $(N_t\lambda_\pi)^2$ and $(N_e\lambda_{p\sigma})^2$ can shortly be written as[31]

$$A_p = C(R) + \left[\frac{(N_e\lambda_{p\sigma})^2}{3} - \frac{(N_t\lambda_{p\pi})^2}{4}\right]\frac{A_p^0}{5}. \tag{6}$$

Here $C(R)$ involves the so-called metal-metal and metal-ligand contributions which are mainly dependent upon R. The last contribution directly reflects the covalency where the quantity $A_p^0 = 1280$ MHz corresponds to free F^- ion. Using the values of $(N_t\lambda_\pi)^2$ and $(N_e\lambda_{p\sigma})^2$ given in Table V and assuming that $C(R)$ is the same for both systems an increase in A_p of about 4 MHz can be estimated from Eq. (6) on going from $KMgF_3:Mn^{2+}$ to $LiBaF_3:Mn^{2+}$. Therefore, the difference between $A_p = 11 \pm 0.1$ MHz for $LiBaF_3:Mn^{2+}$ and the figures (in the range 8–9 MHz) measured for Mn^{2+} in normal perovskites (Table I) can be associated with an increase in covalency consistent with the calculated values of Table V.

Calculated values of the HF constant, A, in the 2.02 Å $\leq R \leq 2.10$ Å range are also collected in Table VI. For both $KMgF_3:Mn^{2+}$ and $LiBaF_3:Mn^{2+}$, A is found to be negative and slightly dependent upon R. Both facts reflect that for an octahedral d^5 complex with $S = 5/2$ in the ground state the isotropic HF constant A arises from the polarization of $1s$, $2s$, and $3s$ *core* levels by the five unpaired d electrons.[39] By this reason it is more difficult to reproduce the A value than the anisotropic SHF constant A_p coming essentially from e_g and t_{2g} *valence* orbitals. Despite this fact the calculations give for $LiBaF_3:Mn^{2+}$ an A value which is about 8 MHz smaller than that for $KMgF_3:Mn^{2+}$ and thus it is in agreement with the trend displayed by experimental A values (Table I).

The difference between the A values for $KMgF_3:Mn^{2+}$ and $LiBaF_3:Mn^{2+}$ can again be ascribed mainly to a slightly different bonding in the two systems.[55] Assuming, in a simple model, that A reflects the unpaired spin density lying onto the Mn^{2+} impurity, A can be written as
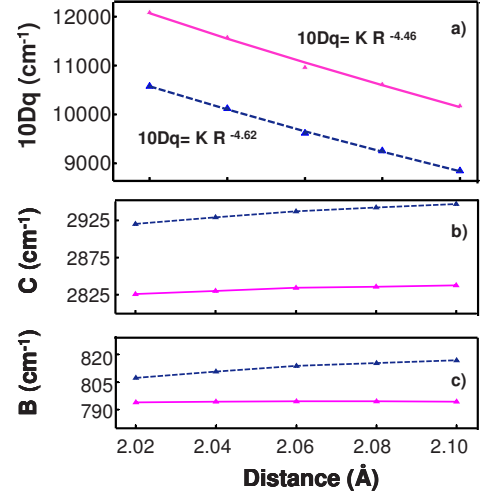
$$A = \frac{2N_e^2 + 3N_t^2}{5}A_0, \tag{7}$$

where A_0 refers to free Mn^{2+} ion. Using Eq. (7) and the calculated N_t^2 and N_e^2 values of Table IV it is found $A(KMgF_3:Mn^{2+})/A(LiBaF_3:Mn^{2+}) = 1.04$ which is not far from the figure $A(KMgF_3:Mn^{2+})/A(LiBaF_3:Mn^{2+}) = 1.08$ derived from the calculations as it is shown in Table VI.

D. 10Dq and the $^6A_1(t_{2g}^3e_g^2) \rightarrow {}^4A_{1g}, {}^4E_g(t_{2g}^3e_g^2)$ transition energy

In this section the 10Dq values calculated for both $KMgF_3:Mn^{2+}$ and $LiBaF_3:Mn^{2+}$ as a function of the Mn^{2+}-F^- distance, R, are shown together with the corresponding values of the Racah parameters, B and C, derived through the LFDFT method.[51] For checking the reliability of this method, the *free* Mn^{2+} ion has firstly been studied. After calculating the energy of 252 Slater determinants the values of Racah parameters $B_0 = 958$ cm^{-1} and $C_0 = 3438$ cm^{-1} for free Mn^{2+} have been obtained. These values are thus not far from the corresponding figures $B_0 = 960$ cm^{-1} and $C_0 = 3325$ cm^{-1} derived from experimental optical transitions.[1]

Main results derived for $KMgF_3:Mn^{2+}$ and $LiBaF_3:Mn^{2+}$ are displayed in Fig. 2. In accord with previous calculations[53,54] B and C are found to be very little dependent on R for the two explored systems. So, in the range 2 Å $< R <$ 2.1 Å $|\Delta B/B|$ is found to be smaller than 1.5%. By contrast, results on Fig. 2 point out that 10Dq is strongly dependent upon R. The variation of calculated 10Dq values around $R_I = 2.06$ Å follow the pattern of Eq. (3) with the exponent n being close to 4.5 for *both* $KMgF_3:Mn^{2+}$ and $LiBaF_3:Mn^{2+}$ systems. It is worth noting that the figure obtained for $KMgF_3:Mn^{2+}$ essentially coincides with the value $n = 4.7$ measured for MnF_6^{4-} embedded in a series of normal perovskites.[6,7] This fact stresses that when electrons are actually localized on a MX_N complex the changes on electronic
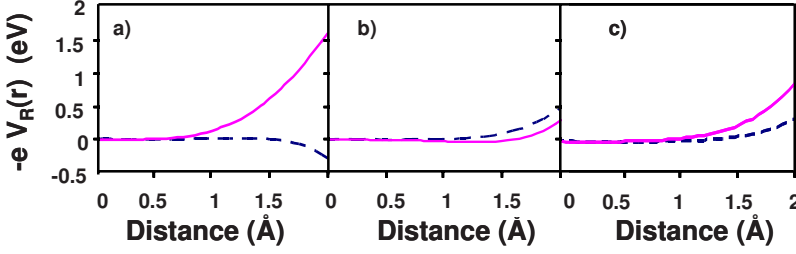
FIG. 3. (Color online) a) Electrostatic potential, $V_R(\mathbf{r})$, of the rest of lattice ions on a MnF_6^{4-} complex depicted along $\langle 100 \rangle$ type directions for $LiBaF_3$ (solid line) and $KMgF_3$ (dashed line). b) The same for $\langle 110 \rangle$ type directions. c) The same for $\langle 210 \rangle$ type directions.

properties induced by the different chemical pressures of iso-morphous host lattices are the same than those produced by a hydrostatic pressure applied to one of the systems. This statement is, however, no longer true when vibrational properties are considered.[35,40,56] The origin of the strong dependence of 10Dq upon R has previously been discussed.[57,58]

Despite the calculated values $n = 4.46$ for $LiBaF_3 : Mn^{2+}$ and $n = 4.62$ for $KMgF_3 : Mn^{2+}$ are very similar, the 10Dq value itself is found to be clearly higher for the former system than for the latter. For instance, at $R = 2.06$ Å we obtain $10Dq = 10961$ and 9610 cm^{-1} for $LiBaF_3 : Mn^{2+}$ and $KMgF_3 : Mn^{2+}$, respectively, as it is shown in Table III. This pattern is thus consistent with the experimental $E_3 - E_1$ values given in Table II and with the figures $10Dq = 9795$ cm^{-1} for $LiBaF_3 : Mn^{2+}$ and $10Dq = 8430$ cm^{-1} for $KMgF_3 : Mn^{2+}$ extracted from measured crystal-field transitions (Table III). In the same vein results gathered in Fig. 2 show that B and C are a little smaller for MnF_6^{4-} in $LiBaF_3$ than in $KMgF_3$.

The values of crystal-field transitions calculated by the LFDFT method[51] for both $KMgF_3 : Mn^{2+}$ and $LiBaF_3 : Mn^{2+}$ are displayed in Table III and compared to experimental findings. It can be noted that the main experimental features are reproduced by the present calculations. So, the energy of the first $^6A_{1g}(t_{2g}^3 e_g^2) \rightarrow {}^4T_{1g}(t_{2g}^4 e_g^1)$ transition calculated for MnF_6^{4-} in $LiBaF_3$ is found to be 2000 cm^{-1} smaller than in $KMgF_3$, while the calculated values for the sharp $^6A_{1g}(t_{2g}^3 e_g^2) \rightarrow {}^4A_{1g}, {}^4E_g(t_{2g}^3 e_g^2)$ transition ($E_3 = 22815$ and 22120 cm^{-1} for $KMgF_3 : Mn^{2+}$ and $LiBaF_3 : Mn^{2+}$, respectively) follow the trend exhibited by the corresponding experimental values $E_3 = 25200$ and 24096 cm^{-1}. This difference can again mainly be ascribed to a different chemical bonding in the two considered systems reflected in Table V. In a simple model the E_3 value can be approximated by[59]

$$E_3 = E_3^0 N_e^2 N_t^2, \tag{8}$$

where E_3^0 refers to free Mn^{2+} ion. According to this simple view and the N_e^2 and N_t^2 values displayed in Table V, a ratio $E_3(KMgF_3 : Mn^{2+}) / E_3(LiBaF_3 : Mn^{2+}) = 1.09$ is derived which can be compared with the experimental value (Table III) equal to 1.05.

E. Microscopic origin of the differences between $LiBaF_3 : Mn^{2+}$ and $KMgF_3 : Mn^{2+}$

The analysis carried out in the preceding sections supports that the observed differences when comparing optical and magnetic parameters of $LiBaF_3 : Mn^{2+}$ and $KMgF_3 : Mn^{2+}$ cannot be ascribed mainly to distinct R_I values. By contrast, such an analysis stress that although R_I is practically the

same for both systems the unpaired electrons spend more time on F^- ligands in $LiBaF_3 : Mn^{2+}$ than in $KMgF_3 : Mn^{2+}$. Bearing in mind that antibonding e_g and t_{2g} electrons are essentially *localized* in the MnF_6^{4-} complex such a difference can be related to a different internal electric field, $\mathbf{E}_R$, due to all lattice ions lying *outside* the complex.

A direct proof of the relevance of $\mathbf{E}_R(\mathbf{r})$ is obtained through calculations on an *isolated* MnF_6^{4-} complex with $R_I = 2.06$ Å though subject to the internal electric field corresponding to $LiBaF_3$ or $KMgF_3$ lattices. For the SHF constant, a value $A_p = 6.2$ MHz is found for the *in vacuo* MnF_6^{4-} complex, while a close value $A_p = 7.4$ MHz is obtained when the electric field $\mathbf{E}_R(\mathbf{r})$ corresponding to the $KMgF_3$ lattice is added in the calculation. By contrast, the calculated A_p value for MnF_6^{4-} under the internal field of $LiBaF_3$ is found to be equal to 10.9 MHz thus implying that $A_p(LiBaF_3 : Mn^{2+}) - A_p(KMgF_3 : Mn^{2+}) \cong 3$ MHz. These results are thus similar to those collected in Table VI. A similar situation is encountered for A and 10Dq parameters. In fact the A and 10Dq values calculated for a simple MnF_6^{4-} complex under $\mathbf{E}_R(\mathbf{r})$ are close to those derived by means of a 21 ion cluster for $LiBaF_3 : Mn^{2+}$ and $KMgF_3 : Mn^{2+}$ (Tables III and VI).

The differences in $\mathbf{E}_R(\mathbf{r})$ for $LiBaF_3$ and $KMgF_3$ lattices can be understood displaying the associated potential $V_R(\mathbf{r})$ with $\mathbf{r}$ along $\langle 100 \rangle$, $\langle 110 \rangle$, and $\langle 210 \rangle$ directions (Fig. 3). According to the local O_h symmetry, at the Mn^{2+} site $\mathbf{E}_R = 0$. However, this is no longer true for a ligand site whose local symmetry is only C_{4v}. As shown in Fig. 3, when $\mathbf{r}$ runs along a $\langle 100 \rangle$ direction $(-e) V_R(\mathbf{r})$ *increases* significantly on passing from the Mn^{2+} site to the ligand place for the $LiBaF_3$ host lattice. By contrast, in the case of $KMgF_3$ $(-e) V_R(\mathbf{r})$ is constant on going from $(0,0,0)$ to $(1.5,0,0)$ Å. It is worth noting that $V_R(\mathbf{r})$ is nearly flat for *both* types of lattices when $\mathbf{r}$ runs along a $\langle 110 \rangle$ direction. However, when $\mathbf{r}$ is parallel to $\langle 210 \rangle$ $(-e)$, $V_R(\mathbf{r})$ shows a significant raising near to the ligand site for $LiBaF_3$ but not again for $KMgF_3$.

In agreement with Eq. (5), the antibonding e_g ($\sim x^2 - y^2$, $3z^2 - r^2$) electrons spend some time on ligands. Moreover, the electronic density associated with this orbital is primarily lying around $\langle 100 \rangle$ directions and thus the effect of $(-e)$ $V_R(\mathbf{r})$ tends to raise such levels in the case of $LiBaF_3$ host lattice in comparison to $KMgF_3$.[46] By contrast, the effect of $(-e)$ $V_R(\mathbf{r})$ on π t_{2g} ($\sim xy, xz, yz$) orbitals (mainly directed toward $\langle 110 \rangle$ directions) is expected to be much smaller according to Fig. 3. This reasoning is thus able to explain albeit qualitatively why 10Dq is bigger for $LiBaF_3 : Mn^{2+}$ than for $KMgF_3 : Mn^{2+}$ (Tables II and III) despite R_I is found to be practically the same for both systems (Table IV). In other words, 10Dq does not depend on the actual R_I value but *also* on the shape of $V_R(\mathbf{r})$. To formulate more precisely this idea

let us call $[10Dq(R)]_v$ the 10Dq value expected for a complex *in vacuo*. When the complex is inserted in a lattice there is, however, a *supplementary* contribution to 10Dq,[21,46] coming from $V_R(\mathbf{r})$, which shall be designated as Δ_R. Therefore the actual 10Dq value can simply be written as

$$10Dq = [10Dq(R)]_v + \Delta_R. \tag{9}$$

If, *around* R_I, $[10Dq(R)]_v$ follows a law

$$[10Dq(R)]_v = K_v R^{-n} \tag{10}$$

and if $\Delta_R \ll [10Dq(R_I)]_v$, then the R dependence of 10Dq on R is given by Eq. (3) but the K constant does depend on Δ_R through the expression

$$K \simeq K_v \left(1 + \frac{\Delta_R}{K_v R_I^{-n}} \right). \tag{11}$$

This simple reasoning thus explains the main differences between the R dependence of 10Dq values calculated for LiBaF$_3$:Mn^{2+} and KMgF$_3$:Mn^{2+}. Such differences are portrayed in Fig. 2. Therefore, as K is sensitive to the form of $V_R(\mathbf{r})$ it may happen that if a complex is placed in two different lattices and R_I is the same, both systems do not have necessarily the same 10Dq value.

Let us now focus on the influence of $V_R(\mathbf{r})$ on bonding. Looking at the shape of $(-e) V_R(\mathbf{r})$ along a $\langle 100 \rangle$ direction in LiBaF$_3$ and in KMgF$_3$ (Fig. 3) it is clear that $V_R(\mathbf{r})$ favors an *additional* net flow of σ electrons from ligands to Mn^{2+} in the case of LiBaF$_3$:Mn^{2+}. Care has to be taken, however, to understand properly the mechanism responsible for this flow. In complexes *in vacuo* such as MnF$_6^{4-}$ (with ligands with closed-shell structure) 3d orbitals are lying above $2p(F^-)$ orbitals and there is a net flow of electronic charge from ligands to the central cation which is the only one allowed by the Pauli principle.[1,3,40] Despite this fact unpaired electrons in antibonding levels (coming from 3d levels of free cation) spend some time on ligands as a result of the $3d(\text{Mn}^{2+})$ $-2p(F^-)$ admixture [Eqs. (4) and (5)]. However, in the counterpart bonding levels (coming from $2p(F^-)$ levels of free anion) there is also a partial transfer of electronic charge to the central cation fostered by the $3d(\text{Mn}^{2+})-2p(F^-)$ admixture. As in the ground state of transition-metal complexes (such as MnF$_6^{4-}$ or CrF$_6^{4-}$) bonding levels are fully populated while there are holes in antibonding levels this implies that the net flow of electronic charge goes from ligands to the central cation.

Bearing in mind this reasoning it can now be understood that the action of the $(-e) V_R(\mathbf{r})$ term in LiBaF$_3$:Mn^{2+} along $\langle 100 \rangle$ directions tends to decrease the separation between mainly $3d(\text{Mn}^{2+})$ and mainly $2p(F^-)$ orbitals and thus to enhance the probability of finding an antibonding e_g electron on ligands. This explains qualitatively the differences between $(N_e)^2$ and $(N_e \lambda_{p\sigma})^2$ for LiBaF$_3$:Mn^{2+} and KMgF$_3$:Mn^{2+} displayed on Table V.

Finally, it is crucial to understand the quite different behavior of $V_R(\mathbf{r})$ in the normal and in the inverted perovskite. As both lattices are cubic $V_R(\mathbf{r})$ can be written as

$$V_R(\mathbf{r}) = \sum_i V_i(\mathbf{r}). \tag{12}$$

Here $V_i(\mathbf{r})$ means the contribution of the i shell (involving ions all of them placed at a distance R_i from Mn^{2+}) displaying an O_h symmetry. Therefore, in a multipolar expansion of $V_i(\mathbf{r})$ around $\mathbf{r}=0$ the first nonconstant contribution depends on R_i^{-5}.[1,3] For this reason, important differences in the shape of $V_R(\mathbf{r})$ for the normal and the inverted perovskite already appear considering only the first two shells ($i=1,2$) lying outside the MnF$_6^{4-}$ complex.[46] In both KMgF$_3$ and LiBaF$_3$ lattices (Fig. 1) the first shell is composed by a cube of eight cations with charge Z_1 lying at a distance $R_1=\sqrt{3}R_0$ from the origin, while the second shell is formed by an octahedron of cations with charge Z_2 placed at distance $R_2=2R_0$. According to crystal-field theory the contributions, $V_1(\mathbf{r})$ and $V_2(\mathbf{r})$, arising form the first and second shell can be written as

$$V_1(\mathbf{r}) = V_1^0 + \alpha \frac{8}{9} \frac{Z_1}{R_1^5} \left(x^4 + y^4 + z^4 - \frac{3}{5} r^4 \right) + \dots$$

$$V_2(\mathbf{r}) = V_2^0 - \alpha \frac{Z_2}{R_2^5} \left(x^4 + y^4 + z^4 - \frac{3}{5} r^4 \right) + \dots \tag{13}$$

Here $\alpha > 0$ and V_1^0 and V_2^0 are constants. Therefore, if $V_R(\mathbf{r}) \approx V_1(\mathbf{r}) + V_2(\mathbf{r})$ then $V_R(\mathbf{r})$ can be approximated by

$$V_R(\mathbf{r}) \approx V_1^0 + V_2^0 + \frac{\alpha}{R_0^5} \frac{\Sigma(Z_1;Z_2)}{7776} \left(x^4 + y^4 + z^4 - \frac{3}{5} r^4 \right) + \dots \tag{14}$$

Here the $\Sigma(Z_1;Z_2)$ function is defined by

$$\Sigma(Z_1;Z_2) = 256\sqrt{3}Z_1 - 243Z_2 \tag{15}$$

The $\Sigma(Z_1;Z_2)$ quantity plays a key role for explaining the differences between the shape of $V_R(\mathbf{r})$ in the normal and inverted perovskite lattices.[46] For a normal perovskite $Z_1 =1$ and $Z_2=2$ implying $\Sigma(Z_1;Z_2)=-42.6$. By contrast, in an inverted perovskite $Z_1=2$ and $Z_2=1$ and then $\Sigma(Z_1;Z_2) =643.8$ which is thus about 15 times higher than the absolute value of $\Sigma(Z_1;Z_2)$ calculated for the normal perovskite. This just means that in the inverted perovskite the effects of the first shell composed by *divalent* Ba^{2+} ions dominate over those coming from the second one involving *monovalent* ions and placed further. By contrast, in a normal perovskite such as KMgF$_3$ the effect due to Mg^{2+} ions in the second shell practically cancels $V_1(\mathbf{r})$ coming from first K$^+$ ions thus giving rise to a $V_R(\mathbf{r})$ function which is essentially constant over the complex region.

V. FINAL REMARKS

Although active electrons of a transition-metal impurity, M, placed in an insulating lattice are usually localized in the MX$_N$ complex the present results stress the key role played by the internal electric field, $\mathbf{E}_R$, for properly understanding both the chemical bonding inside the complex and the related EPR and optical parameters. The influence of this field which appears inevitably in any insulating compound with ionic

character is not considered within the traditional LFT. In particular, the study carried out in this work demonstrates that the influence of $\mathbf{E}_R$ can not be avoided when comparing the properties of the same complex in two nonisomorphous host lattices *even* if both are cubic. The present conclusion has thus some relation with the nearsightedness principle.[60] In short, the electronic density in a small region is only affected by what happens in a neighbor buffer region as well as by the long-range Coulomb potential due to all ions which are necessarily formed in insulators with a partial ionic bonding.

According to the present study $\mathbf{E}_R$ not only affects 10Dq but every property associated with the embedded complex. For this reason the energy of charge-transfer transitions in $LiBaF_3:Mn^{2+}$ and $KMgF_3:Mn^{2+}$ are not necessarily equal. Let us consider the separation between the nonbonding t_{1g} orbitals (mainly built from $2p(F^-)$ orbitals) and the antibonding t_{2g} ($\sim xy, xz, yz$) orbitals. It is found in the present calculations that such a separation is 2400 cm^{-1} smaller for $LiBaF_3:Mn^{2+}$ than for $KMgF_3:Mn^{2+}$, a fact which partially reflects the raising of $2p(F^-)$ orbitals in the former system due to the shape of $V_R(\mathbf{r})$ depicted in Fig. 3. Unfortunately, there are up to now no experimental information on charge-transfer transitions of the present systems[2,61,62] lying in the vacuum UV region. The influence of $V_R(\mathbf{r})$ upon charge transfer transitions has been well demonstrated for $NH_4X:Cu^{2+}(X=Cl,Br)$ where such transitions appear in the optical domain.[63] Furthermore, very recently[64] it has been shown that the energy of the first charge transfer transition corresponding to $Be_3Si_6Al_2O_{18}:Fe^{3+}$ is about 1700 cm^{-1} smaller than that for $Al_2O_3:Fe^{3+}$. This difference has also been interpreted as the result of distinct $V_R(\mathbf{r})$ potential in beryl and corundum host lattices.

The form of $V_R(\mathbf{r})$ inside the complex region is described but approximately by Eq. (14) thus implying that $V_R(\mathbf{r})$ is positive when $\mathbf{r}$ is parallel to $\langle 100 \rangle$ directions but negative when $\mathbf{r}$ runs along a $\langle 111 \rangle$ direction. Bearing in mind this fact, it is worth remarking here that the importance of $V_R(\mathbf{r})$ is enhanced due to the directionality of orbitals. Indeed the electronic density in e_g and t_{2g} orbitals is not isotropically distributed in the complex but is mainly lying around $\langle 100 \rangle$ and $\langle 110 \rangle$ type directions, respectively.

Through the present study it is confirmed that a good starting point for understanding the properties of a transition-metal impurity in insulators is to consider only the complex at the right experimental distance, R_I, and subject to the internal electric field, $\mathbf{E}_R$. This supports the explanation on the actual origin of the different color displayed by ruby and emerald.[20,21] Along this line the present results stress that when the same complex in two different host lattices displays a different 10Dq value this fact does not necessarily mean that the equilibrium distance, R_I, is not the same. This conclusion is thus in contradiction with what is usually assumed within the traditional LFT.

The analysis performed in this work suggests that changes in bonding should appear when comparing ruby and emerald simply as a result of a different internal electric field. As in the ground state of a CrO_6^{9-} complex there are only three antibonding electrons in the t_{2g} orbital, changes in bonding are in principle expected to be smaller than for the present systems where there are two additional electrons placed in the antibonding e_g orbital which has a σ character. Apart from this reason the study in the two referred gemstones is not simple due to the low local symmetry which is only C_3 for ruby. Work along this direction is planned for a near future.

[1] J. S. Griffith, *The Theory of Transition-Metal Ions* (Cambridge University Press, Cambridge, 1961).

[2] C. K. Jörgensen, *Modern Aspects of Ligand Field Theory* (North-Holland, Amsterdam, 1971).

[3] S. Sugano, Y. Tanabe, and H. Kamimura, *Multiplets of Transition-Metal Ions in Crystals* (Academic, New York, 1970), Vol. 33, p. 331.

[4] S. Darwish and M. S. Seehra, Phys. Rev. B **37**, 3422 (1988).

[5] V. Goldberg, R. Moncorge, D. Pacheco, and B. DiBartolo, *Luminescence of Inorganic Solids* (Plenum, New York, 1988).

[6] M. C. Marco de Lucas, F. Rodríguez, and M. Moreno, Phys. Rev. B **50**, 2760 (1994).

[7] F. Rodriguez, M. Moreno, A. Tressaud, and J. P. Chaminade, Cryst. Lattice Defects Amorphous Mater. **16**, 221 (1987).

[8] M. T. Barriuso, J. A. Aramburu, and M. Moreno, J. Phys.: Condens. Matter **11**, L525 (1999).

[9] B. Villacampa, R. Cases, V. M. Orera, and R. Alcala, J. Phys. Chem. Solids **55**, 263 (1994).

[10] J. A. Aramburu, J. I. Paredes, M. T. Barriuso, and M. Moreno, Phys. Rev. B **61**, 6525 (2000).

[11] C. M. de Lucas, F. Rodríguez, J. M. Dance, M. Moreno, and A. Tressaud, J. Lumin. **48-49**, 553 (1991).

[12] M. T. Barriuso and M. Moreno, Chem. Phys. Lett. **112**, 165 (1984).

[13] F. Rodriguez, I. Hernandez, M. Moreno, and R. Alcala, J. Chem. Phys. **119**, 8686 (2003).

[14] O. S. Wenger, R. Valiente, and H. U. Gudel, J. Chem. Phys. **115**, 3819 (2001).

[15] J. M. García-Lastra, M. Moreno, and M. T. Barriuso, J. Chem. Phys. **128**, 144708 (2008).

[16] R. G. Burns, *Mineralogical Applications of Crystal Field Theory* (Cambridge University Press, Cambridge, 1993).

[17] R. C. Powell, *Physics of Solid State Laser Materials* (Springer, New York, 1998).

[18] E. Gaudry, A. Kiratisin, P. Sainctavit, C. Brouder, F. Mauri, A. Ramos, A. Rogalev, and J. Goulon, Phys. Rev. B **67**, 094108

(2003).

[19] E. Gaudry, D. Cabaret, C. Brouder, I. Letard, A. Rogalev, F. Wilhlem, N. Jaouen, and P. Sainctavit, Phys. Rev. B **76**, 094110 (2007).

[20] J. M. García-Lastra, M. T. Barriuso, J. A. Aramburu, and M. Moreno, Phys. Rev. B **72**, 113104 (2005).

[21] J. M. García-Lastra, J. A. Aramburu, M. T. Barriuso, and M. Moreno, Phys. Rev. B **74**, 115118 (2006).

[22] T. Yosida, H. Aoki, H. Takeuchi, M. Arakawa, and K. Horai, J. Phys. Soc. Jpn. **46**, 1661 (1979).

[23] T. Yosida, J. Phys. Soc. Jpn. **49**, 127 (1980).

[24] S. Ogawa, J. Phys. Soc. Jpn. **15**, 1475 (1960).

[25] T. P. P. Hall, W. Hayes, J. Wilkens, and R. W. Stevenson, J. Chem. Phys. **38**, 1977 (1963).

[26] R. K. Jeck and J. J. Krebs, Phys. Rev. B **5**, 1677 (1972).

[27] J. J. Rousseau, A. Leble, and J. C. Fayet, J. Phys. (Paris) **39**, 1215 (1978).

[28] M. E. Ziaei, Can. J. Phys. **59**, 298 (1981).

[29] H. Aoki, M. Arakawa, and T. Yosida, J. Phys. Soc. Jpn. **52**, 2216 (1983).

[30] P. Studzinski and J. M. Spaeth, J. Phys. C **19**, 6441 (1986).

[31] M. T. Barriuso, J. A. Aramburu, M. Moreno, M. Florez, G. F. Rodrigo, and L. Pueyo, Phys. Rev. B **38**, 4239 (1988).

[32] B. Henke, M. Secu, U. Rogulis, S. Schweizer, and J. M. Spaeth, Phys. Status Solidi C **2**, 380 (2005).

[33] D. Babel and A. Tressaud, in *Inorganic Solid Fluorides*, edited by P. Hagenmuller (Academic, New York, 1985).

[34] S. Haussühl, K. Recker, and R. Leckebus, Z. Naturforsch. A **27**, 1022 (1972).

[35] M. T. Barriuso, M. Moreno, and J. A. Aramburu, Phys. Rev. B **65**, 064441 (2002).

[36] N. Sarukura, H. Murakami, E. Estacio, S. Ono, R. El Ouenzerfi, M. Cadatal, T. Nishimatsu, N. Terakubo, H. Mizuseki, Y. Kawazoe, A. Yoshikawa, and T. Fukuda, Opt. Mater. (Amsterdam, Neth.) **30**, 15 (2007).

[37] M. Nikl, E. Mihóková, Z. Málková, A. Vedda, M. Martini, K. Shimamura, and T. Fukuda, Phys. Rev. B **66**, 184101 (2002).

[38] B. Henke, U. Rogulis, and S. Schweizer, J. Phys.: Condens. Matter **18**, 1577 (2006).

[39] A. Abragam and B. Bleaney, *Electron Paramagnetic Resonance of Transition Ions* (Clarendon, Oxford, 1970), p. 911.

[40] M. Moreno, M. T. Barriuso, J. A. Aramburu, P. García-Fernández, and J. M. García-Lastra, J. Phys.: Condens. Matter **18**, R315 (2006).

[41] M. T. Barriuso, J. A. Aramburu, and M. Moreno, J. Mol. Struct.: THEOCHEM **537**, 117 (2001).

[42] J. A. Aramburu, M. Moreno, and M. T. Barriuso, J. Phys.: Condens. Matter **4**, 9089 (1992).

[43] M. G. Brik and K. Ogasawara, Phys. Rev. B **74**, 045105 (2006).

[44] M. Duarte, E. Martins, S. L. Baldochi, S. P. Morato, N. D. Vieira, and M. M. F. Vieira, Opt. Commun. **151**, 366 (1998).

[45] M. Mortier, B. Piriou, J. Y. Buzaré, M. Rousseau, and J. Y. Gesland, Phys. Rev. B **67**, 115126 (2003).

[46] J. M. García-Lastra, J. Y. Buzaré, M. T. Barriuso, J. A. Aramburu, and M. Moreno, Phys. Rev. B **75**, 155101 (2007).

[47] G. te Velde, F. M. Bickelhaupt, E. J. Baerends, C. F. Guerra, S. J. A. Van Gisbergen, J. G. Snijders, and T. Ziegler, J. Comput. Chem. **22**, 931 (2001).

[48] A. D. Becke, Phys. Rev. A **38**, 3098 (1988).

[49] J. P. Perdew, Phys. Rev. B **33**, 8822 (1986).

[50] A. G. Piken and W. van Gool, Ford Motor Company Technical Report No. SL 68-10, 1968; Program modified by J. A. Aramburu, 1996.

[51] M. Atanasov, C. A. Daul, and C. Rauzy, Chem. Phys. Lett. **367**, 737 (2003).

[52] C. T. Lee, W. T. Yang, and R. G. Parr, Phys. Rev. B **37**, 785 (1988).

[53] M. Florez, L. Seijo, and L. Pueyo, Phys. Rev. B **34**, 1200 (1986).

[54] V. Luaña, M. Bermejo, M. Florez, J. M. Recio, and L. Pueyo, J. Chem. Phys. **90**, 6409 (1989).

[55] E. Simanek and K. A. Muller, J. Phys. Chem. Solids **31**, 1027 (1970).

[56] J. M. García-Lastra, T. Wesolowski, M. T. Barriuso, J. A. Aramburu, and M. Moreno, J. Phys.: Condens. Matter **18**, 1519 (2006).

[57] M. Moreno, J. A. Aramburu, and M. T. Barriuso, Phys. Rev. B **56**, 14423 (1997).

[58] P. García-Fernández, J. M. García-Lastra, J. A. Aramburu, M. T. Barriuso, and M. Moreno, Chem. Phys. Lett. **426**, 91 (2006).

[59] D. Curie, C. Barthou, and B. Canny, J. Chem. Phys. **61**, 3048 (1974).

[60] W. Kohn, Phys. Rev. Lett. **76**, 3168 (1996).

[61] S. Hirako and R. Onaka, J. Phys. Soc. Jpn. **51**, 1255 (1982).

[62] J. Simonetti and D. S. McClure, J. Chem. Phys. **71**, 793 (1979).

[63] J. A. Aramburu and M. Moreno, Phys. Rev. B **56**, 604 (1997).

[64] G. Spinolo, I. Fontana, and A. Galli, Phys. Status Solidi B **244**, 4660 (2007).